Received: 23 September 2020 | Revised: 29 January 2022 | Accepted: 15 February 2022

DOI: 10.1002/joc.7585

RESEARCH ARTICLE

International Journal of Climatology RMetS

Improved spring temperature reconstruction using earlywood blue intensity in southeastern China

Xinguang Cao[1,2] | Hongbing Hu[1] | Pei-ken Kao[1] | Brendan M. Buckley[3] | Zhipeng Dong[2] | Xiuling Chen[2] | Feifei Zhou[2] | Keyan Fang[2]

[1]College of Geography and Tourism, Huanggang Normal University, Huanggang, China

[2]Key Laboratory of Humid Subtropical Eco-Geographical Process (Ministry of Education), Fujian Normal University, Fuzhou, China

[3]Tree-Ring Laboratory, Lamont-Doherty Earth Observatory, Columbia University, Palisades, New York, USA

Correspondence
Keyan Fang, Key Laboratory of Humid Subtropical Eco-Geographical Process (Ministry of Education), Fujian Normal University, Cangshan Campus, Fuzhou 350007, China.
Email: kfang@fjnu.edu.cn

Funding information
Lamont Center for Climate and Life; Open Project of Dabie Mountain Tourism Economy and Culture Research Center, Key Research Base of Humanities and Social Sciences in Hubei Province (2021); Science and Technology Research Project of Hubei Provincial Department of Education, Grant/Award Number: B2020164; Youth Talent Support Program of Fujian Province, Grant/Award Number: IRTL1705; Natural Science Foundation Project of Fujian Province, Grant/Award Number: 2017J0101; State Administration of Foreign Experts Affairs of China, Grant/Award Number: GS20190157002; National Youth Talent Support Program of China (Ten Thousand People Plan); Strategic Priority Research Program of the Chinese Academy of Sciences, Grant/Award Number: XDB26020000; National Science Foundation of China, Grant/Award Numbers: 1602629, 41772180, 41888101, 41822101, 41971022

Abstract

Because instrumental observations are too short to fully represent long-term natural variability, high-resolution temperature proxy records are essential to understanding past climate and assessing current climate variability in the context of long-term patterns. In the subtropics, progress in this field has been hampered by a relative lack of long and truly temperature-sensitive proxy records. In this study, we provide an assessment of the dendroclimatic potential of blue intensity (BI) and ring-width (RW) measurements from two hot/humid *Pinus massoniana* sites in China. Our results show that RW exhibits a significant ($p < .05$) response to precipitation over a hydrological year (previous November to October) and to temperature over the winter–spring season (January to March). We find the earlywood blue intensity parameter to be the most robust parameter for reconstruction purposes; over the 1916–2015 period, it explains 36% of regional-scale spring season (March–May) temperature variance. Strong agreements between the current reconstruction and observed temperature over a large area of southeastern China implied that our reconstruction exhibited high reliability and large spatial representation. As expected, our reconstructed temperature data are directly correlated with El Niño–Southern Oscillation. These results suggest that there is great potential to use BI to advance our understanding of temperature variability in regions hot and humid climate regimes. However, more studies are needed to understand (1) which subtropical tree species will be appropriate for use and (2) how to overcome biases from differential staining between sapwood and heartwood.

KEYWORDS

blue intensity (BI), ENSO, humid subtropical China, temperature reconstruction, tree ring

1 | INTRODUCTION

Current warming trends are particularly pronounced over high latitudes (e.g., the Arctic; Serreze and Barry, 2011), high altitudes (e.g., the Tibetan Plateau; Pepin *et al*., 2015), and semi-arid regions (e.g., the semi-arid regions of Central Asia; Huang *et al*., 2012 and North America; Heeter *et al*., 2021). Warming is less pronounced over the hot and humid tropics and subtropics (IPCC, 2014). Proxy-based reconstructions reveal more divergent temperature variations across regions relative to the current warming (Neukom *et al*., 2019), highlighting the need for temperature reconstructions over different regions. Most tree-ring records sensitive to temperature are found in high latitudes/elevations (Jacoby *et al*., 1996; Büntgen *et al*., 2006; Yadav *et al*., 2011; Tingley and Huybers, 2013; Popa and Bouriaud, 2014), whereas proxy reconstructions in the tropics and subtropics are scarce. Similarly, most of the terrestrial proxy archives from these regions yield information about hydroclimate rather than temperature (Rossi *et al*., 2006; Schongart *et al*., 2006; Sano *et al*., 2009; Buckley *et al*., 2010; Buckley *et al*., 2017), thereby limiting our ability to study the temperature linkages between cold/arid regions and hot/humid regions.

In China, most temperature reconstructions have been published for western China, where the climate is cold and arid (e.g., Liang *et al*., 2008; Zhu *et al*., 2008; Fan *et al*., 2009; Duan *et al*., 2010; Wang *et al*., 2015; Liang *et al*., 2016). Studies in the subtropical areas of China (e.g., Duan *et al*., 2012; Chen *et al*., 2012a, 2012b; Duan *et al*., 2013) are relatively underdeveloped so far. In subtropical China, forest in that area with better hydrothermal conditions and more serious human disturbance, which makes the research difficult. However, the area with dense population and rapid economic development, frost damage has a strong impact on socioeconomic activities (Shi *et al*., 2010) and the occurrence of consecutive coldness events has received great attention from climate researchers (Duan *et al*., 2012). Temperature in southeastern China is strongly influenced by atmosphere–ocean variability in the Asian-Pacific region (e.g., the El Niño–Southern Oscillation [ENSO]; East Asian Summer Monsoon [EASM]; and the Pacific Decadal Oscillation [PDO]) (Macdonald and Case, 2005; D'Arrigo and Wilson, 2006; Zhou *et al*., 2009; Chen *et al*., 2012a; Wang *et al*., 2018). Temperature reconstructions in southeastern China provide key information about historical variations and their co-variability with large-scale temperature variations and linkages with oceanic and atmospheric modes (Shi *et al*., 2010, 2015; Duan *et al*., 2012; Chen *et al*., 2012a, 2012b; Cai and Liu, 2013; Duan *et al*., 2013). However, much effort is needed to develop temperature reconstructions over key regions that currently lack such information.

Tree rings are the most widely used proxy for high-resolution temperature reconstructions (Esper *et al*., 2002; Cook *et al*., 2004; Moberg *et al*., 2005; D'Arrigo *et al*., 2006). Among the tree-ring proxies used for climate reconstruction, the density parameter has been widely shown to be more temperature-sensitive than other proxies, namely ring width (RW) (e.g., Anchukaitis *et al*., 2013, 2017; Esper *et al*., 2015; Li *et al*., 2015, 2017; Liang *et al*., 2016). McCarroll *et al*. (2002) found that measuring the intensity of the reflected blue portion of the light spectrum from scanned images of wood samples (known as blue intensity [BI]) provides a less costly and less time-consuming alternative to X-ray densitometry. Björklund *et al*. (2013) suggested that BI, typically from the latewood (LW) portion of the annual growth ring, provides a reliable density proxy that can be used for temperature reconstruction. In the last two decades, BI has been widely used for temperature reconstruction in Europe (e.g., Björklund *et al*., 2014; Björklund *et al*., 2015; Rydval *et al*., 2016; Fuentes *et al*., 2017; Rydval *et al*., 2017; Wilson *et al*., 2017), North America (e.g., Wilson *et al*., 2014; Wilson *et al*., 2017; Heeter *et al*., 2020), and Southeast Asia. In 2018, Buckley et al. published the first use of BI from a tropical region, measuring BI from the earlywood (EWBI) and latewood (LWBI) of *Fokienia hodginsii*. In 2020, Cao et al. presented the first tree-ring BI chronology from a low elevation site (100–260 m.a.s.l., 152 years) in humid subtropical China. Both studies indicate the strong potential for BI-based reconstruction in tropical and subtropical regions. However, no specific BI-based temperature reconstruction has been published in hot and humid southeast China to date.

EWBI is a less-explored tree ring parameter; more studies are needed to evaluate its utility for different tree species and regions (Buckley *et al*., 2018; Cao *et al*., 2020; Seftigen *et al*., 2020). As with LWBI, the greatest limitation of EWBI is that any colour variation that is not representative of climatic processes affecting cell wall thickness will bias the resultant raw reflectance measurements. For example, some conifer species (e.g., *Pinus massoniana*) show a clear, sharp colour change from the lighter sapwood (SW) to darker heartwood (HW), which induces low-frequency-related colour intensity biases. To reduce the effect of differences in colour within a tree, samples to be used for BI analysis are refluxed with ethanol or acetone before being scanned (Campbell *et al*., 2011). Nevertheless, these differences impose a systematic change in reflectance around the HW/SW transition (Björklund *et al*., 2014, 2015; Rydval *et al*., 2014).

In this paper, we build upon previous climate response research (Guo *et al*., 2018; Wang *et al*., 2018) and measure BI variables (including EWBI, LWBI and delta BI) from two sites in southeast China. The objectives of this study are to: (1) assess the dendroclimatic potential of these parameters by evaluating the strength and temporal stability of their seasonal climate signal; (2) estimate the historical temperature reconstruction possibilities of tree ring BI parameters; and (3) explore tempo-spatial models of temperature reconstruction. We also explore and the mechanisms related to the atmospheric-ocean teleconnections and interactions with remote oceans.

2 | MATERIALS AND METHODS

2.1 | Study sites

Our study area comprises two *P. massoniana* sites in Fujian Province in southeastern China: Makeng (site code MK, 25.57°N, 117.35°E) and Fangguangyan (site code FGY, 25.88°N, 119.18°E) (Figure 1). The study area is characterized by a subtropical monsoon climate. Monthly mean temperature (Temp) and monthly total precipitation (Precip) values were obtained from three nearby meteorological stations: FuZhou (119.28°E, 26.08°N, 84 m a.s.l., 1953–2015 AD), Yong'an (117.35°E, 25.97°N, 206 m a.s.l., 1953–2015 AD), and Xianyou (118.70°E, 25.37°N, 77 m a.s.l., 1957–2015 AD). These climate data were provided by the National Meteorological Information Center (http://data.cma.cn; Table S1, Figure 1). Instrumental data indicate that the local climate is characterized by monthly average temperatures ranging from 10.4°C in January to 28.1°C in July. Precipitation ranges from 38.2 mm in December to 235.3 mm in June (averaged over the period 1953–2015) and the annual mean air temperature and sum of precipitation are 19.5°C and 1,471.9 mm, respectively. Although the total annual precipitation is high, relatively little of it falls during the summer growing season due to the strength of the Western Pacific High. Therefore, trees often experience drought stress during the summer months (Chen *et al.*, 2016; Li *et al.*, 2016).

2.2 | Tree-ring data and chronology development

BI measurements were made on core samples collected over the past few years from living *P. massoniana* trees. At each site, two to three tree-ring cores were taken at breast height. From an overall collection of 56 (142) cores taken from 34 (78) trees at the MK (FGY) site, we selected 39 (92) core samples from 28 (66) trees from which to obtain BI measurements. The selection criterion was the absence of a continuous blue fungal stain. We also excluded cores if they possessed excessive amounts of traumatic resin ducts across the entire radial width of an annual ring because failure to avoid such cellular abnormalities results in inaccurate blue reflectance values. The reduction of the selected sample size has little impact on the quality of the chronology, as the RW time series developed from the subset correlate significantly with the original growth index (r = .95 for MK and r = .98 for FGY, respectively; Figure S2, Figure S3). Before scanning, all samples were first cross-dated visually using a 40x microscope. Because the *P. massoniana* wood collected at these sites is characterized by a dark colour and generally exhibits discoloration due to differences in the HW/SW or resins, chemical pigment extraction was required for our samples. Such extraction is

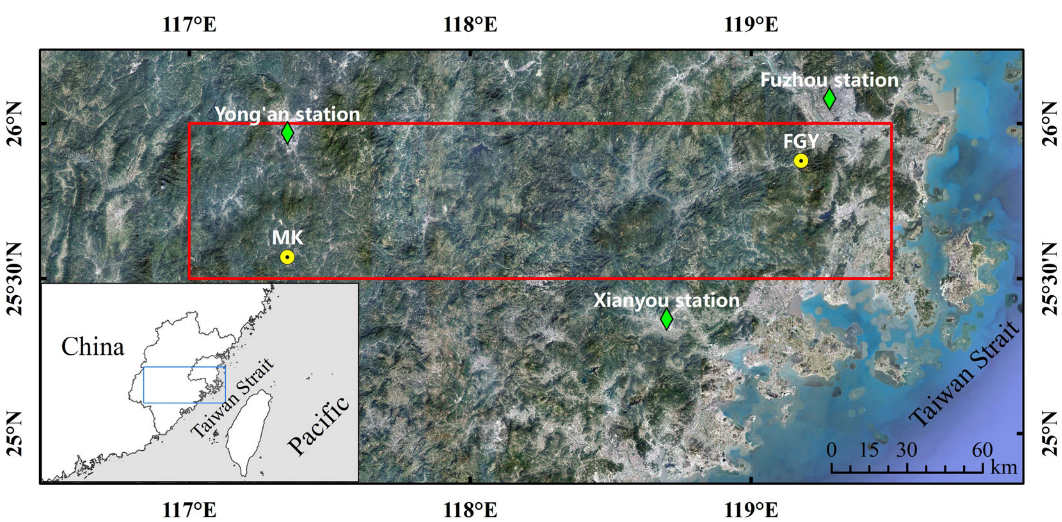

FIGURE 1 Locations of the tree-ring sites used in this study (yellow dots; Table S1). Also indicated (red line box) is the domain (25.5–26°N, 117–119.5°E) of the gridded data (CRU TS 4.04, Harris *et al.*, 2020) used for calibration and the three weather stations used in this paper (green rhombi) [Colour figure can be viewed at wileyonlinelibrary.com]

often necessary when using the BI methodology (Björklund *et al*., 2014; Rydval *et al*., 2014). A mixture of benzene and ethanol (analysis reagent, 2:1) is used for Soxhlet extraction for 48 hours in order to reduce the colour transition between HW and SW, but still some staining can remain (Figure S4). The samples were dried and re-sanded/polished again with 1,200 grit sandpaper after chemical treatment (i.e., they were originally surfaced for RW measurement). We first calibrated our scanner (Epson Perfection V800 Photo) using an IT8.7/2 calibration card to ensure the accuracy of the generated BI values. We then scanned the prepared cores using the flatbed scanner equipped with SilverFast Ai Studio (Version 8.8) software with a resolution of 3,200 dpi resolution (pixel size ∼8 μm). A box with a black-lined inner surface was used during scanning to avoid ambient light biases (Rydval *et al*., 2014).

The image analysis software CooRecorder 9.3 (Larsson, 2018) was used to measure the RW data. After obtaining RW measurements, we checked our dating accuracy using the software COFECHA (Holmes, 1983). Once confident that all samples were accurately dated, we used the software CooRecorder 9.3/CDendro 9.3 (Larsson, 2018) to measure BI from the earlywood (EWBI) and latewood (LWBI). The raw LWBI was defined as the average of the darkest 10% of the pixels in latewood, whereas the EWBI was defined as the average of the lightest 80% of the pixels in earlywood. The trend of the BI reflection value is negatively correlated with the tree-ring density. For consistency with other studies, we inverted our data for EWBI and LWBI by multiplying each value by −1, then added a constant of 2.56 to ensure all inverted values were positive (see Rydval *et al*., 2014). *P. massoniana* is known to have a high resin content that often imparts a marked change in colour at the HW/SW boundary. To account for colour changes in each core that were not adequately removed by the Soxhlet extraction, delta blue intensity (ΔBI) was automatically calculated as the residual of the raw LWBI and EWBI in CooRecorder (Björklund *et al*., 2014).

Standardization is a crucial data processing step in dendroclimatology that aims to remove non-climatic age-related trends while retaining the desired climatic signal (Cook et al., 1990). The RW and BI data were detrended using the ratio between the raw measurements and smoothing splines with a 50% frequency-response cutoff of two-thirds of the series length using the program ARSTAN (Cook and Peters, 1981). These dimensionless tree-ring indices were then compiled into a chronology using the bi-weight robust mean method (Cook, 1985). This standardization option retains the interannual to multi-decadal signals in the time series, while minimizing longer-term frequency biases due to HW–SW colour changes (Seftigen *et al*., 2020). Site- and parameter-level chronologies were produced by averaging the dimensionless indices. A total of 8 chronologies of 4 different tree-ring parameters (RW, EWBI, LWBI, and ΔBI) from 2 sites were included in the new dataset (Figure S5).

We used the running Expressed Population Signal (i.e., EPS) with a 50-year window and 49-year overlap to evaluate the quality of the chronologies over time (Briffa and Jones, 1990), that way we'll get a higher-resolution time series of EPS and see exactly the year at which EPS drops below 0.70. The reliable portion of the chronologies is determined when the EPS $\geq$0.70 (Wigley *et al*., 1984) and replication $\geq$10 series for BI and RW (Table 1). Although an EPS threshold of 0.85 is commonly used, a lower limit of 0.7 was adopted to maximize the useable chronology span. Also, the common regional signal is effectively increased as a result of the utilization of principal component regression rather than utilizing chronologies individually.

2.3 | Climate response and statistical analyses

Principal component analysis (PCA, using a varimax rotation) was performed over the period 1863–2015 for all of the parameter chronologies to assess the coherence between the parameters. Additionally, PCA was performed separately on a parameter-level to summarize the regional common variability of each individual wood component. Time series of PC scores of the first principal components (PC1) were retained for climate response analysis.

The relationship between the time series of the PC scores and the monthly climate variables were investigated via Pearson correlation analyses from the end of the previous growing season in October to the end of the current growing season in December. By including prior season climate we are able to understand the carryover effects of climate from the year prior to growth—a phenomenon common to conifers (Fritts, 1976). On the basis of the correlation analysis of the raw data, we added a first-difference data analysis between proxy and instrumental data. This process removes all variation on the medium- and low-frequency bands to prevent biased correlations due to spurious similarities in trends (Björklund *et al*., 2014). We performed these tests using monthly mean temperature and total precipitation data from the Climatic Research Unit (CRU) TS 4.04 dataset. The data cover the period 1901–2015 and have a 0.5° by 0.5° resolution (Harris *et al*., 2020) in the grid box from 25.5–26.0°N to 117–119.5°E, which includes our sampling sites (Figures 1 and 2). The KNMI Climate Explorer (Trouet and Van Oldenborgh, 2013) was used to assess spatial

TABLE 1 Basic statistics for each site and parameter

	RBar	*n* for EPS (0.70)	Year EPS 0.70	CV	AC1	SNR
RW						
FGY	0.200	10	1859	0.306	0.472	14.994
MK	0.174	11	1799	0.224	0.508	5.877
Mean	0.187	10.5	1829	0.265	0.490	10.436
EWBI						
FGY	0.103	20	1862	0.050	0.266	6.774
MK	0.131	16	1802	0.044	0.353	3.463
Mean	0.117	18	1832	0.047	0.310	5.119
LWBI						
FGY	0.102	21	1862	0.035	0.450	6.689
MK	0.114	18	1807	0.024	0.615	2.966
Mean	0.108	19.5	1834.5	0.030	0.533	4.828
ΔBI						
FGY	0.088	24	1863	0.055	0.447	5.788
MK	0.093	23	1823	0.050	0.666	2.358
Mean	0.091	23.5	1843	0.053	0.557	4.073

Note: n for EPS (0.70) = the number of series needed to acquire an EPS value of 0.70. RW is given in mm; BI is given as the absorbed intensity. Note that BI values were inverted for these calculations.
Abbreviations: AC1, first-order autocorrelation; CV, coefficient of variation (STDEV/MEAN; STDEV: standard deviation, MEAN: mean tree-ring width/blue intensity); EPS, Expressed Population Signal; RBAR, the average correlation coefficient between the detrended series; SNR, signal-to-noise ratio.

correlations between temperature data and RW, EWBI, and ΔBI data.

A simple linear ordinary least squares regression model was employed to reconstruct the optimal season identified by the climate response analysis using the PC composites indices. We split the instrumental period (1916–2015) into two equal periods (the "early" period [1916–1965] and "late" period [1966–2015]) to validate and cross-validate the reconstruction model (Table 2). The verification statistics include the Pearson's correlation coefficient (r), R-squared (R^2), coefficient of efficiency statistic (CE), reduction of error (RE), and the sign test. Positive values of RE and CE indicate the positive predictive skill of the model (Fritts, 1976). We used a longer calibration period of 50 years for the split calibration-verification to ensure that the robustness of the calibration model matched that of previous studies (Fuentes *et al*., 2017; Wilson *et al*., 2017).

We used wavelet analysis to examine the periodic cycles in the reconstructed series (Mann and Lees, 1996; Torrence and Compo, 1998). To understand the background circulation conditions associated with March–May temperature, sea surface temperature (SST) data were obtained from the National Oceanic and Atmospheric Administration Extended Reconstructed Sea Surface Temperature dataset version 5 (ERSSTv5; Huang *et al*., 2017). Atmospheric fields obtained from the

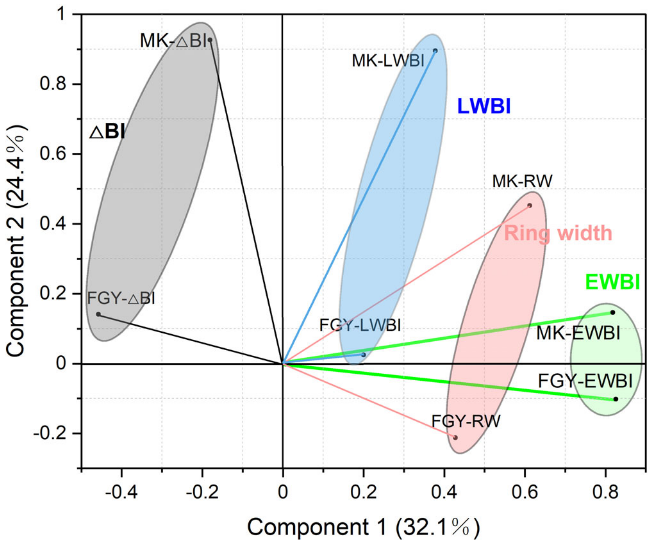

FIGURE 2 Scatter plot of principal component analysis loadings of each chronology on the first two eigenvectors. Identified parameter cohorts are highlighted in different colours. The colour of the vectors corresponds to the different parameters (green lines–EWBI; blue–LWBI; pink–RW; black–ΔBI). The first two components together represent nearly 57% of the total variation. EWBI, earlywood blue intensity; LWBI, latewood blue intensity; RW, ring width; ΔBI, delta blue intensity [Colour figure can be viewed at wileyonlinelibrary.com]

TABLE 2 Calibration and verification results of the model

Validation/cross-validation	C (r/R^2)	V (r/R^2)	CE	RE	Sign test
Early period calibration/late period verification					
Calibration (1916–1965)	0.47***/0.22	-	-	-	36+/14−**
Verification (1966–2015)	-	0.60***/0.36	0.27	0.52	-
Late period calibration/early period verification					
Calibration (1966–2015)	0.60***/0.36	-	-	-	34+/16−*
Verification (1916–1965)	-	0.47***/0.22	0.18	0.43	-
Full period (1916–2015)	0.59***/0.35	-	-	-	66+/34−**

Note: ***$p < .001$; **$p < .01$; *$p < .05$.
Abbreviations: CE, coefficient of efficiency statistic; R, correlation coefficient; R^2, explained variance; RE, reduction of error statistic.

National Center for Environmental Prediction–National Center for Atmospheric Research (NCAR/NCEP) Reanalysis (Kalnay *et al.*, 1996) were also used in the present analyses. In addition, the monthly Niño 3.4 index (retrieved from https://climatedataguide.ucar.edu/climate-data/nino-sst-indices-nino-12-3-34-4-oni-and-tni) was used to explore the possible impact of remote oceans on March–May temperature in southeastern China.

3 | RESULTS AND DISCUSSION

3.1 | Chronology signals

FGY contains 92 series spanning the period 1854–2015, whereas MK is comprised of 39 series and spans the period 1785–2015 (Table S1). For each individual site, the RW chronology shows higher inter-sequence coefficients of variation (mean CV = 0.265; Table 1) than the BI chronologies (mean CV = 0.043, ranging from 0.030–0.053). A low degree of variation for BI series relative to RW series is also found in other studies in high latitudes (e.g., Wilson *et al.*, 2014). This may be because the BI series are often more sensitive to temperature but tend to show a lower degree of sensitivity to precipitation (e.g., McCarroll *et al.*, 2013; Björklund *et al.*, 2014; Fuentes *et al.*, 2017; Rydval *et al.*, 2017; Wilson *et al.*, 2017). The signal-to-noise ratio (SNR) is higher for RW series (mean SNR = 10.436) than for BI series (mean SNR = 4.673, ranging 4.073–5.119) (Table 1). In addition, mean inter-series correlation (RBAR) values indicate that RW maintains the strongest common signal. Relatively low SNR and RBAR mean that more samples are needed to obtain a reliable chronology. Time series of BI have commonly exhibited lower common signals relative to RW (e.g., Wilson *et al.*, 2017; Buckley *et al.*, 2018; Blake *et al.*, 2020). This reflects the lower variability of BI, as indicated by a lower CV relative to that of RW. The first-order autocorrelation (AC1) of the RW series is higher than that of EWBI. A high AC1 indicates a strong impact of previous growth on current growth and a high portion of low-frequency signals. Relatively high autocorrelation/persistence is, however, also true for tree-ring widths more generally and is not restricted to conifers. However, it may be worth noting that BI series often exhibit considerably lower autocorrelation compared to TRW series (Rydval *et al.*, 2014; Fuentes *et al.*, 2016; Fuentes *et al.*, 2017). As shown in Table 1, this also appears to be the case for EWBI. It is quite interesting that the LWBI/ΔBI have higher AC1 than RW, although the difference is not large. One likely contributor to this effect is the previously noted HW–SW bias that could still exist in EWBI series even after Soxhlet extraction has been performed. However, the HW-SW bias has little effect on the latewood series of *P. massoniana* due to its darker color. In addition, this may be related to the negative correlation between LWBI/ΔBI and temperature at low latitudes (Cao *et al.*, 2020；Buckley *et al.*, 2018), which different from the positive response at high latitudes (Rydval *et al.*, 2014; Fuentes *et al.*, 2016; Fuentes *et al.*, 2017). We emphasize that this work is an isolated case; this issue requires further attention before it can be assumed that this applies more generally.

For each individual site, tree-ring metrics of RW and EWBI across each site correlate strongly with each other, while ΔBI has the weakest coupling with RW and all BI metrics, followed by LWBI (Table S2). Strong, positive correlations ($p < .001$) between metrics across different sites suggest a strong spatial correspondence between overall growth and physiological response of same-species individuals at closely situated sites.

To further examine the relationships between the various tree-ring parameters, a rotated varimax PCA was performed on all eight parameter chronologies over their common period (1863–2010). Figure 2 presents the bivariate scatter plot of each parameter chronology on the first two eigenvectors. The first two eigenvectors of PCA explain 32.1 and 24.4% of the total variability, respectively. PC1 is dominated by both the EWBI and RW chronologies, which cluster together in the bivariate plot. However, the loadings of the RW chronologies are obviously weaker on PC1 than those of

EWBI. The LWBI and ΔBI components are partially separated from the RW and EWBI clusters, and the ΔBI appears in a separate quadrant in the PCA bivariate plot. Moreover, ordination of the two components shows a complete separation of ΔBI from the rest of the chronologies, with the former having lesser influences on PC1 but strong and positive loadings on PC2. ΔBI shares a negative loading on this axis and is thus negatively correlated with EWBI, as indicated by the ~120° angle between the respective vector cohorts. These results show an obvious common signal in the dataset, but there are also suggest the presence of distinct signal patterns. We analysed this signal structure through climate sensitivity analysis, and further explored the inter-parameter consistency of variability.

3.2 | Climate-growth relationship

PCA (1863–2015) was rerun on the chronologies of EWBI, RW, and each tree-ring parameter in the full network. Pearson correlations between monthly climate variables and first principal component scores (PC1) of tree-ring parameters are summarized in Figure 3. The leading PC for EWBI, RW, LWBI, and ΔBI parameters account for 75.767.253.5and 56.4% of the total variability, respectively, and for approximately 42.0% when all sites and parameters are combined.

The correlations with both temperature and precipitation reveal inconsistent parameter response patterns. Temperature dominates the climate signal, as evinced by the strong correlations with temperature in one or several months between previous December and May (Figure 3). All parameters except ΔBI display positive correlations with growing season temperature. EWBI exhibits a stronger significant correlation with temperature than do RW and LWBI, particularly for the mean temperature from March to May for both the non-transformed series ($r = .59$, $p < .01$) and the time-series have been transformed to first differences ($r = .56$, $p < .01$) (Figure 3a,b; Table S3). Potential alternative seasonal windows were also examined (e.g., C1-C5 or C3-C6) and that these alternative seasonal window responses are included in Table S3. The correlation pattern for RW/LWBI is similar to that for EWBI, but the time window is earlier/later

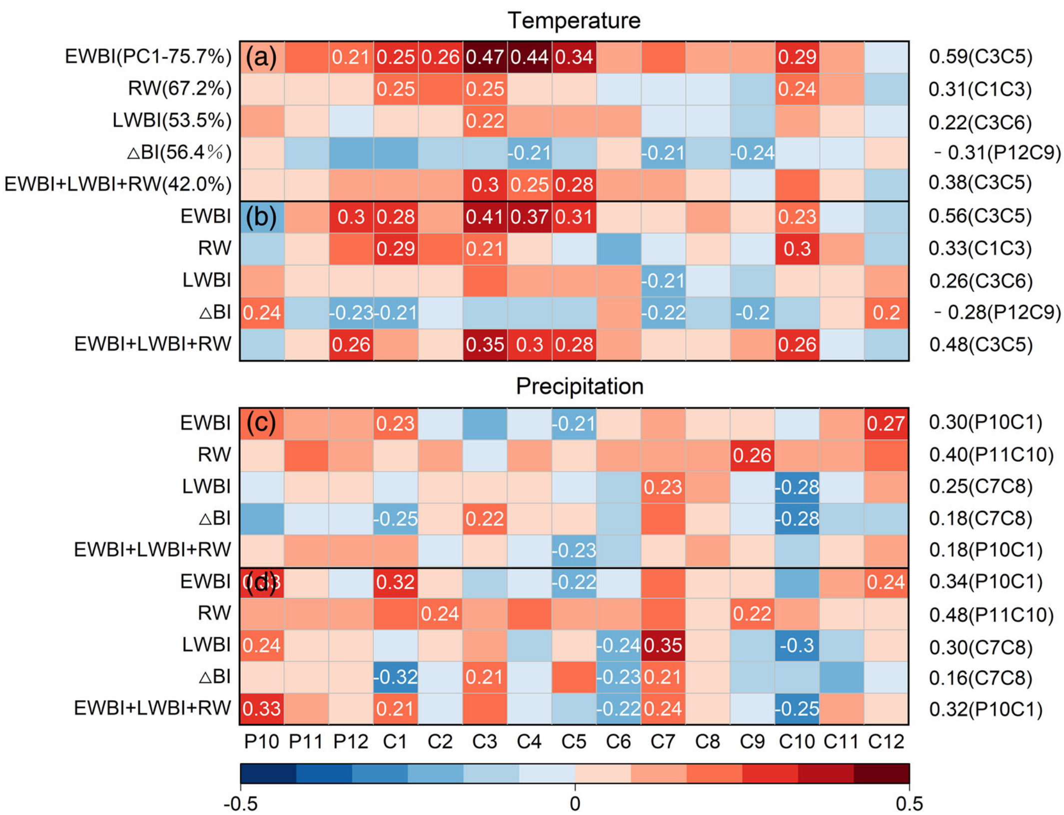

FIGURE 3 Summary for the significant correlations of the PC1 scores for each tree-ring parameter with their corresponding nearest regional (25.5–26°N/117–119.5°E) CRU TS 4.04 gridded variables. Correlations are computed over the 1916–2015 period: (a) and (c) are correlations using non-transformed series, (b) and (d) are correlations after the time-series have been transformed to first differences. The numbers in the parentheses denote the amount of variation explained by the first PC component. Coefficients on the right axis of the plot are peak correlations with seasonally averaged climate variables. Correlations significant at the 95% confidence level are marked in the figure. C, current year; P, previous year [Colour figure can be viewed at wileyonlinelibrary.com]

and the correlation is weaker (C1–C3 $r = .31$ for RW PC1 and C3-C6 $r = .22$ for LWBI PC1, respectively; Figure 3a, Table S3). The spatial correlation fields also indicate that EWBI (Figure 4a) has a considerably stronger correlation with temperature than does RW (Figure 4b). The ΔBI is negatively correlated with temperature (P12-C9 $r = -.31$ for ΔBI PC1, $p < .01$). This pattern is also relatively stable for correlations with first-differenced data (P12-C9 $r = -.28$ for ΔBI PC1), suggesting a moisture limitation caused by increased temperatures. Notably, the correlations between different parameters and October temperature are more like statistical correlations, considering that the continuous formation of different ring components should correspond to the growing season time window. Potential alternative seasonal windows were also examined (e.g., C1-C5 and C3-C6); these seasonal window responses are included in Table S3.

Correlations with precipitation (Figure 3c,d) are weaker and less stable within the regional PC1 variants. Significant ($p < .05$) correlations with precipitation were only found in some scattered months (e.g., January, March, July, and September). Notably, RW was significantly and positively correlated with the precipitation of a hydrological year from previous November to current October ($r = 40$, $p < .001$). This finding indicates that the moisture limitation of a hydrological year for tree growth can also been observed in a humid region if the site is well-drained. EWBI and RW show positive lagged responses with prior year precipitation. Except for ΔBI, no parameters show a significant lagged correlation with temperature in the prior year.

Previous studies of xylogenesis in *P. massoniana* from nearby sites show that cell formation and transformation starts around the middle of March and ends in November (Yang, 2021). The results of this study and those of

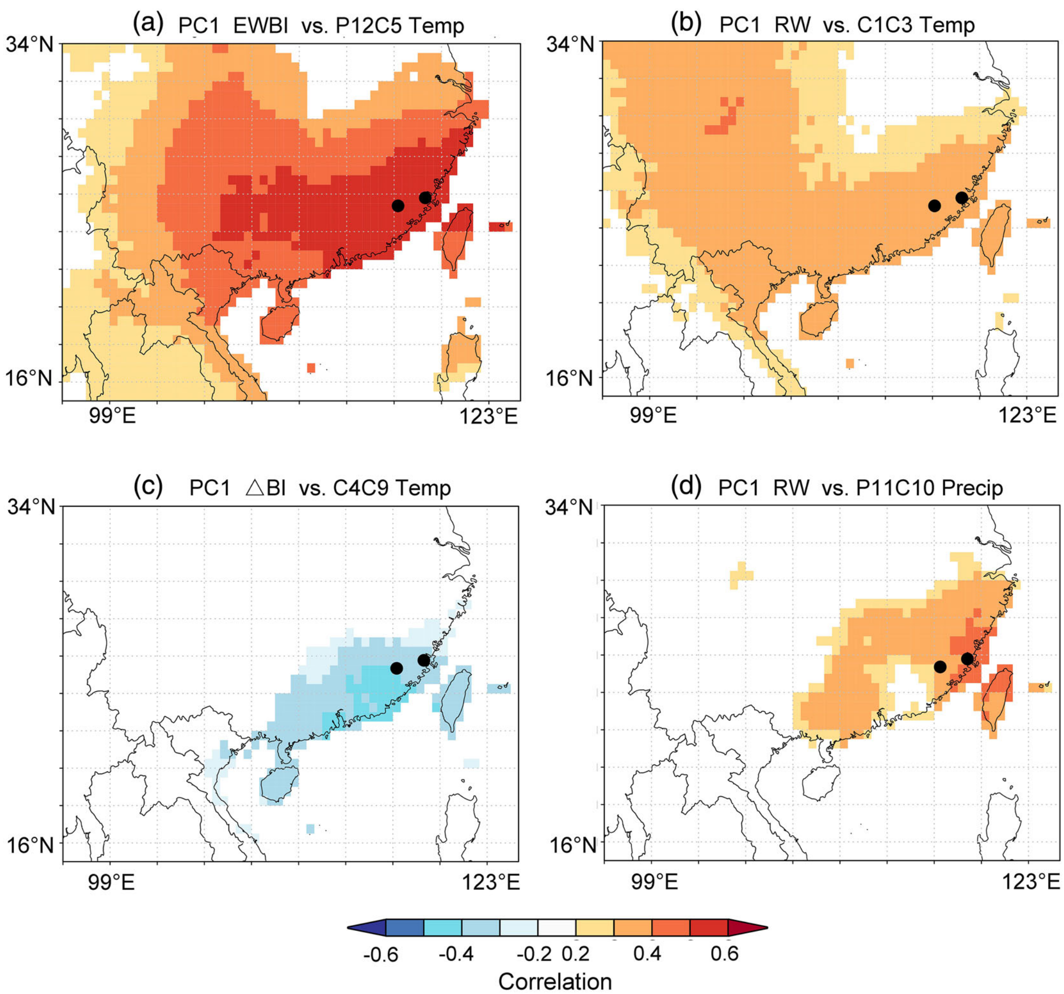

FIGURE 4 Field correlations between selected PC1 composite chronologies and gridded meteorological data from the CRU TS 4.04 product over the 1916–2015 period. (a) Earlywood blue intensity (EWBI) versus March–May temperature (temp); (b) ring width (RW) versus January–March temperature; (c) delta blue intensity (ΔBI) versus previous December to current September temperature; (d) RW versus previous November to current October precipitation (Precip). Black solid circles indicate the locations of the two tree-ring sampling sites. Correlations are shown in colour if significant ($p < .05$) [Colour figure can be viewed at wileyonlinelibrary.com]

studies from ecologically and climatologically similar locations in Fuzhou (e.g., Zhang *et al.*, 2016) show that the formation of latewood occurs between the end of June and early July and mid-November. It can be inferred that earlywood tracheids develop from March to May, which is why EWBI correlates well with climatic conditions during this period. ΔBI captures a longer time window because it includes information from the whole ring (Björklund *et al.*, 2014).

The weak temperature signal of LWBI and ΔBI found here differs from LWBI/ΔBI signals found in higher latitude, conifer-dominated boreal forests in North America and Europe (e.g., Björklund *et al.*, 2013, 2014; Wilson *et al.*, 2014, 2017; Fuentes *et al.*, 2017; Rydval *et al.*, 2017), where LWBI/ΔBI is more significantly positively correlated with temperature than EWBI. The strong positive correlations between our EWBI data and temperature are in agreement with those of other studies in central southeastern Vietnam (Buckley *et al.*, 2018), southeastern China (Cao *et al.*, 2020), and southern and central Sweden (Seftigen *et al.*, 2020). This suggests that a winter/spring temperature limitation on EWBI formation is common to these humid areas. Previous studies have demonstrated that earlywood density is determined by tracheid size (Björklund *et al.*, 2017), which is optimized for efficient water transport (Wodzicki, 1971; Tyree and Zimmermann, 2002). According to the cohesion-tension theory (Angeles *et al.*, 2004; Cochard, 2006), as water evaporates from the leaves, hydraulic tension (i.e., negative pressure) pulls up the entire water column due to the huge cohesive strength of water (Cochard *et al.*, 2013). It is imperative for survival that this water column remains intact. The water column can be cut off during severe droughts, causing complete tree mortality from cavitation. Fortunately, plants have evolved extreme embolism resistance through a variety of physiological responses (Larter *et al.*, 2017). Although spring precipitation in our study area is relatively high (Figure S1), higher temperatures and reduced moisture availability could have a negative effect on earlywood cell enlargement through increased lignification of cell walls in seasonally dry environments at lower latitudes (e.g., this study; Buckley *et al.*, 2018). In these instances, smaller lumen may help prevent cavitation by reducing tension (Larter *et al.*, 2017) and may also yield a higher observed density (i.e., a higher EWBI value).

3.3 | Time stability of the climate response

We assessed the temporal stability of relationships between EWBI, RW, and ΔBI and gridded meteorological temperature data from the CRU TS 4.04 product over the period 1916–2015 using a 31-year moving correlation window. Results are shown in Figure 5 and Figure S6.

Moving correlation analyses indicate that the relationships between EWBI and spring (C3–C5) temperatures are strong over the test instrumental period, although there are slight differences in the seasonal timing of the climate response window. Additionally, the EWBI metric shows significant positive correlations with January and February temperature in the more recent decades (1970–present) (Figure 5). This trend warrants further examination, as it may have important implications regarding the increasingly earlier onset of winter warming in the region. Changes in the seasonal timing due to rapidly warming winter temperatures in the latter half of the twentieth century are well documented in instrumental data across the subtropical China (estimated slopes = 0.03; not shown). Future studies examining the temperature sensitivity of the EWBI parameter therefore warrant additional consideration (Heeter *et al.*, 2019).

RW generally shows a weaker and more temporally unstable relationship with temperature than does EWBI over the test period (Figure S6a). However, RW does show a significant ($p < .05$) positive correlation with January and March temperature in more recent decades. RW also shows a significant positive relationship with October temperature in the late instrumental period (1970–2010). We suspect that the weak and unstable RW-temperature signal is partially due to the presence of the strong precipitation signal in the RW PC1 composites (Figure 3). These data suggest that warmer-than-average winter–spring temperatures could have an increasingly positive effect on the overall radial growth of *P. massoniana* in this region (Duan *et al.*, 2012). They also suggest that RW is not an adequate parameter for capturing and preserving a temperature signal in this region. Further, the data indicate that precipitation is becoming more of a limiting factor on radial tree growth in this region than has been the case in previous decades. The negative temperature signals in ΔBI are comparatively more unstable. The ΔBI parameter largely loses its sensitivity to temperature during the 1920–1970 interval, yet remains sensitive to previous December to September temperatures after 1970 (Figure S6b). Originally, ΔBI was proposed with the goal of mitigating the influence of colour transitions between HW and SW and which, attractive to preserve lower-frequency signals in the BI time-series, for example, at centennial to multi-centennial time-scales (Björklund *et al.*, 2014, 2015; Wilson *et al.*, 2017; Buckley *et al.*, 2018). However, ΔBI in our study have limited climate signals because the correlation between EWBI and LWBI is high (Table S2), which may remove climate-related signals.

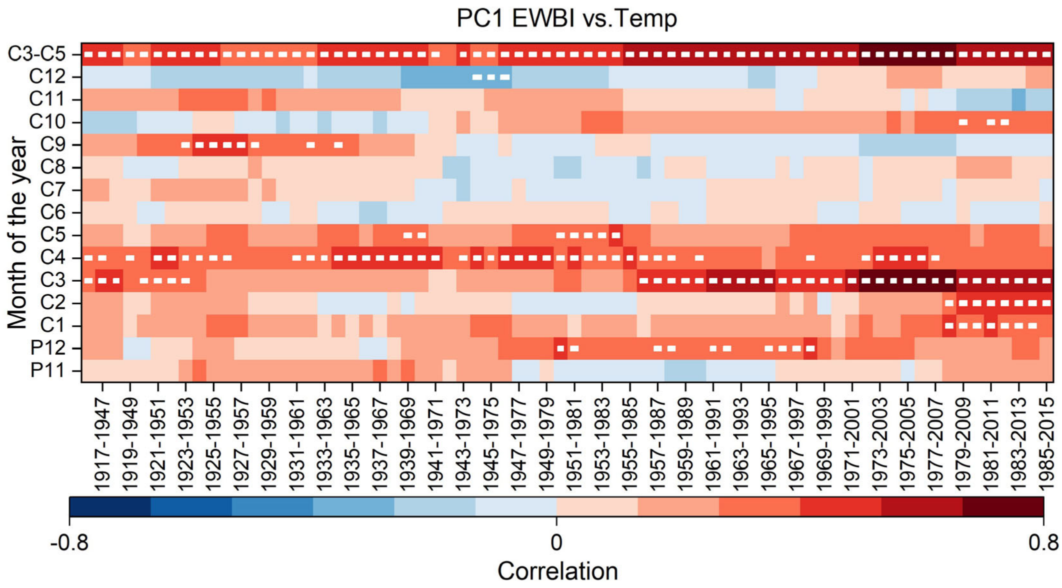

FIGURE 5 Moving 31-year window correlations (white rectangles represent $\alpha = 0.05$) over the 1916–2015 period between selected PC1 EWBI composite chronologies and gridded meteorological temperature data from the CRU TS 4.04 product. Temperature data averaged over the region are bounded by the latitude/longitude coordinates 25.5–26°N/117–119.5°E. EWBI, earlywood blue intensity [Colour figure can be viewed at wileyonlinelibrary.com]

3.4 | Regional temperature reconstruction

Compared to other tree-ring metrics explored in this study, EWBI shows the strongest, steadiest, and most spatially-resolved temperature signal over the entire instrumental period (Figures 4 and 5), therefore we used the EWBI metric for a regionally-averaged spring temperature reconstruction. For comparative purposes, we also include RW, as it can be used as an indicator for hydroclimate variability (Figure S6c,7). A linear regression model was employed to derive a regional temperature reconstruction over the period 1863–2015. The reconstruction model explains 36.0% (R_{adj}^2 = 34.9%) of the instrumental variance for the full calibration period (1916–2015; Table 2). Based on the split-period calibration/verification model, all correlations in different subperiods are significant ($p < .001$) and both early- and late-period (and vice versa) statistics pass the validation tests (Table 2).

Close matches between the actual and estimated data were observed and the reconstructed spring temperature shows a strong correlation with temperature over a large area of southeastern China (Figure 6). This indicates that our results are representative of the temperature and climatic changes in the study area. However, we note that some temperature extremes are underestimated in the estimated series. This may be due to the BI's own limitations. A more detailed assessment by examining metrics assessing the linear trend of the residuals (estimated minus observed data), indicating that the EWBI data cannot well capture the long-term warming trend to some extent. Wilson *et al.* (2014) emphasized the possibility of long-term signal distortion related to detrending options, finding reduced fidelity of LWBI to temperature at frequencies lower than 20 years. Meanwhile, Fuentes *et al.* (2017) argued that the approaches presented in Björklund *et al.* (2014, 2015) allow for the retention of useful low-frequency information when using the ΔBI_{adj} parameter and careful standardization procedures. As of this writing, the use of EWBI is a relatively new method and has only been used to gauge dendroclimatic response in a few sites (e.g., Wilson *et al.*, 2017, 2019; Buckley *et al.*, 2018; Blake *et al.*, 2020; Seftigen *et al.*, 2020). This study is the first to use EWBI metrics to reconstruct temperature in understudied and challenging subtropical conifers, so further experimentation is needed.

The final PC1 EWBI reconstruction of our spring (March–May) mean temperature variability went back from 1863 CE to 2015 CE (Figure 7a). The reconstructed temperature varied between 16.59 and 19.30°C, with a mean value of 17.84°C. The ten coldest years over the past 153 years occurred in 1940 CE, 1927, 1918, 1939, 1938, 1870, 1932, 1869, 1928 and 1968 (starting from the coldest year), whereas the ten warmest years appeared in 1987 CE, 1898, 2002, 2015, 1977, 1972, 2009, 1904, 1882, 1966 and 1902 (beginning with the warmest year). The PC1 EWBI temperature reconstruction and PC1 RW series are further compared with early data from the CRU TS 4.04 product (Figure 7). The correlations

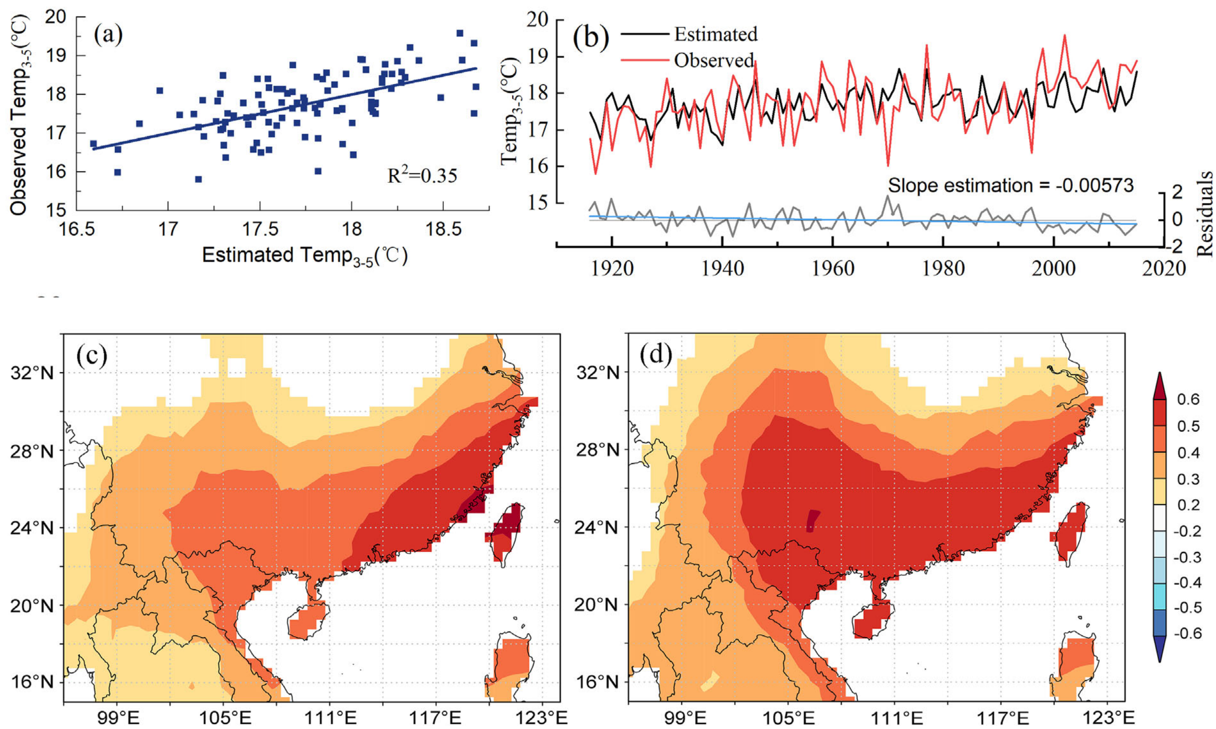

FIGURE 6 (a) Scatter plot of the observed and estimated March–May mean temperatures (Temp$_{3-5}$) during the calibration period 1916–2015; (b) Comparison between observed (red line) and estimated (black line) TMean$_{3-5}$ and the linear trend of the residuals (blue line). Spatial correlation patterns across southeastern China between the (c) non-transformed and (d) first year difference estimated March–May mean temperature and regional CRU TS 4.04 over the period 1916–2015. Correlations are reported in colour if significant ($p < .05$) [Colour figure can be viewed at wileyonlinelibrary.com]

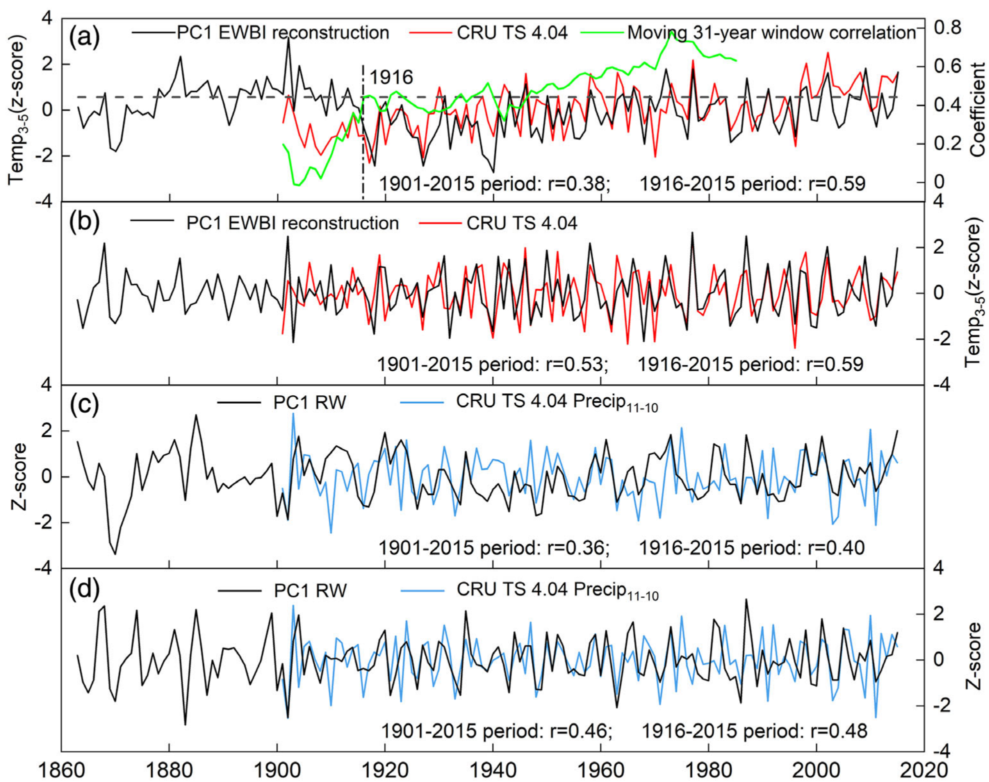

FIGURE 7 Scaled PC1 composite reconstructions and their target CRU TS 4.04 instrumental data. (a and b) EWBI-based March-May temperature (Temp3-5) reconstructions; (c and d) ring width (RW)-based previous November-current October precipitation (Precip11-10) reconstructions. Note that (b and d) data have been high-pass filtered and (a–d) data have been normalized to z-scores over the entire record length. Correlations between time series are provided at the bottom of each plot [Colour figure can be viewed at wileyonlinelibrary.com]

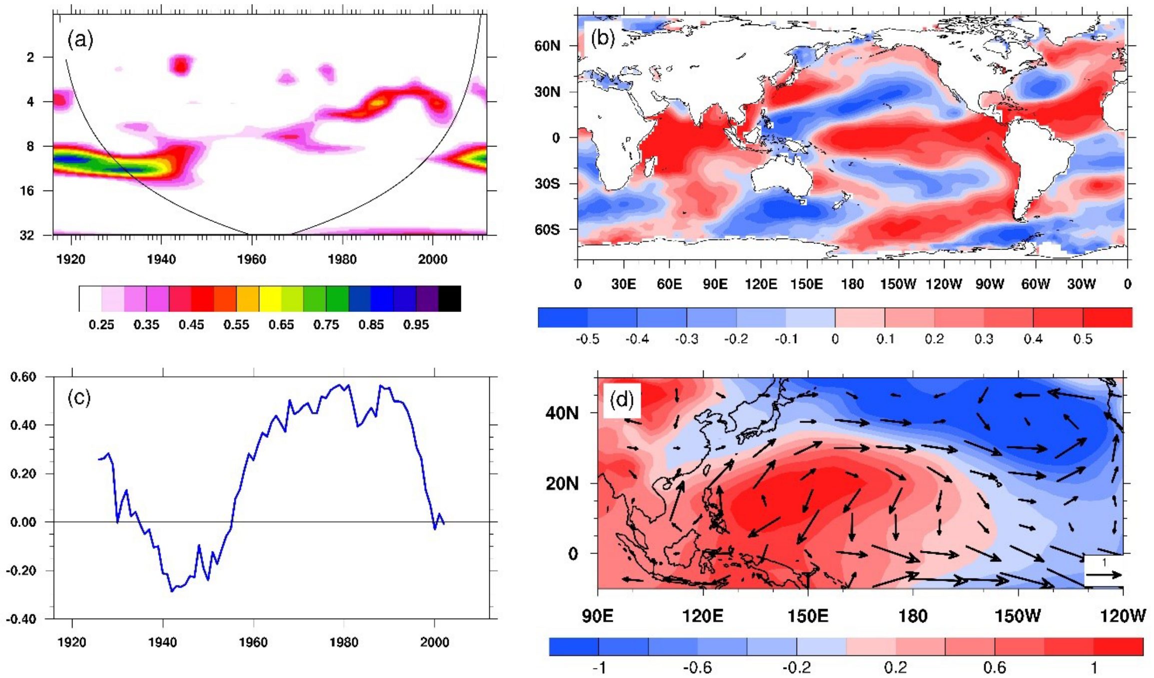

FIGURE 8 (a) Wavelet spectrum of March–May temperature (Temp3–5) reconstruction. (b) Correlation map between the reconstructed temperature and ERSSTv5 during 1965–2000. (c) 21-year sliding correlation coefficients between the $\text{Temp}_{3\text{-}5}$ reconstruction and Niño 3.4 indices. (d) The regression of SLP and 1,000-hPa winds onto the Niño 3.4 index during 1963–1993 [Colour figure can be viewed at wileyonlinelibrary.com]

between the March–May temperature reconstruction and the CRU TS 4.04 instrumental data over the entire observation period (1901–2015) is .38, and .21 lower than the calibration period (1916–2015) (Figure 7a). After high-pass filtering, the correlation coefficients for data from the 1901–2015 period and the 1916–2015 period are almost unanimous (Figure 7b). Correlation coefficients over a moving 31-year window also show that a significant correlation did not exist before 1916 (Figure 7a), suggesting that the early part of the reconstruction is temporally unreliable. The correlation between the unfiltered RW index and historical precipitation observations in the calibration interval (1916–2015) is .40; over the entire common interval (1901–2015), the correlation is .36 (Figure 7c). After high-pass filtering, the correlation coefficients are .48 and .46, respectively (Figure 7d). Despite the limited climate signal of the RW index, it is temporally more stable than EWBI. The temperature response of EWBI exhibits temporal instability outside the calibration interval (1916–2015), which is known as *divergence* (e.g., D'Arrigo *et al.*, 2008). It has been suggested that such decoupling between temperature and EWBI may be the result of abrupt HW/SW colour transitions (Björklund *et al.*, 2019). Rydval *et al.* (2014) highlighted problems with the low-frequency signal of LWBI measured in Scots pine because of the colour differences between HW and SW. The HW/SW offset is visually obvious in the raw *P. massoniana* BI time series (Cao *et al.*, 2020). Thus, this abrupt change is entirely the result of the colour change and not a real change in density. Frustratingly, the existing grease removal and detrending methods have not yet been able to eliminate this bias (e.g., Björklund *et al.*, 2014).

3.5 | Linkage of the $\text{Temp}_{3\text{-}5}$ variations with ENSO

To determine which variables have significant signals in the $\text{Temp}_{3\text{-}5}$, we analysed the spectrum of the $\text{Temp}_{3\text{-}5}$ dataset using wavelet analysis to understand the time-varying frequency. The wavelet analysis revealed that the $\text{Temp}_{3\text{-}5}$ reconstruction is dominated by interannual (∼3–7 year) and interdecadal (8–16 year) variations in which the interannual fluctuation was enhanced and became significant during 1960–2000 (Figure 8a). Because the dominate interannual variation in $\text{Temp}_{3\text{-}5}$ is during this period, a correlation map between $\text{Temp}_{3\text{-}5}$ and SST in March–April–May is shown in Figure 8b. The $\text{Temp}_{3\text{-}5}$ reconstruction is accompanied by an El Niño-like condition—that is, a positive SST anomaly from equatorial eastern to equatorial central Pacific.

To confirm the relationship between $\text{Temp}_{3\text{-}5}$ and El Niño, we calculated the 21-year sliding correlation coefficient between $Temp_{3\text{-}5}$ reconstruction and the Niño 3.4 index (Figure 8c). This enhancement is accompanied by an interdecadal change in the interannual relationship between $Temp_{3\text{-}5}$ reconstruction and the Niño 3.4 index. Since the 1950s, the relationship between $Temp_{3\text{-}5}$ reconstruction and the Niño 3.4 index has become positive. On the basis of the termination of the interannual relationship between $Temp_{3\text{-}5}$ and the Niño 3.4 index during 1963–1993, Figure 8d shows the regression of the Sea Level Pressure (SLP) and 1,000-hPa winds onto the Niño 3.4 index during March–April–May over the period 1963–1993. $Temp_{3\text{-}5}$ is positively correlated with SLP anomalies in the following regions: the North Pacific north of 20°N, the East China Sea from southern Japan to northern Taiwan, and the tropical Southeastern Pacific south of the equator. Conversely, it is positively correlated with SLP anomalies in the Philippine Sea. The particular circulations affecting Fujian are the negative and positive SLP anomalies along the East Asian coast and in the Philippine Sea, respectively. It has been found that the same anti-cyclonic anomalous flow has a great springtime impact over East Asia during El Niño years (Wang *et al*., 2000; Wang and Zhang, 2002; Hung *et al*., 2004). Fujian is west of the anti-cyclonic anomalous flow, the southerly wind anomalies bring warm air from the south (warm advection). When El Niño induces anti-cyclonic circulation in the Philippine Sea, temperatures in Fujian rise.

4 | CONCLUSIONS

In this work, we have described a set of climate responses based on RW, EWBI, LWBI, and ΔBI data measured from two tree-ring sites in Fujian Province, which is located in southeastern China. The results demonstrate that the simple and convenient BI methodology can be used to produce robust temperature-sensitive BI parameters from living *P. massoniana* trees. These findings provide a significant empirical foundation in subtropical low-elevation regions, where few truly temperature-sensitive high-resolution proxy data exist. We explicitly draw attention to the dendroclimatic potential of EWBI because of its sensitivity to temperature. EWBI is a rarely reconstructed climate variable and therefore particularly interesting from a paleoclimate perspective. Although LWBI is commonly used in studies of high-latitude trees, EWBI appears to be most strongly responsive to climate in the current study. We infer that this is the result of hydraulic-functional responses of earlywood in seasonally arid areas to prevent cavitation. The EWBI-derived reconstruction explains 36.0% of the spring temperature and shows that the ENSO is key regulator of March–May temperature in southeastern China. Our work provides the first BI-based temperature reconstruction for the subtropics, which we hope will help to push the boundaries of the BI technique even further.

This research focuses on a single species and a limited region of southeastern China. More research is needed to determine if our findings can be generalized to other subtropical humid regions and for other conifer species. Moreover, the range of measurement biases must be reduced and further studies are needed to overcome offsets related to discolouration and the HW/SW colour transition.

ACKNOWLEDGEMENTS

We are grateful for the constructive comments from two anonymous reviewers. This study was funded by the National Science Foundation of China (41971022, 41822101, 41888101 and 41772180), Strategic Priority Research Program of the Chinese Academy of Sciences (XDB26020000), fellowship for the National Youth Talent Support Program of China (Ten Thousand People Plan), the State Administration of Foreign Experts Affairs of China (GS20190157002), the Natural Science Foundation Project of Fujian Province (2017J0101), fellowship for Youth Talent Support Program of Fujian Province and the innovation team project (IRTL1705). This research was also funded by the Science and Technology Research Project of Hubei Provincial Department of Education (B2020164), and the Open Project of Dabie Mountain Tourism Economy and Culture Research Center, Key Research Base of Humanities and Social Sciences in Hubei Province (2021). Co-author Buckley received funding from NSF Award 1602629, as well as the Lamont Center for Climate and Life.

AUTHOR CONTRIBUTIONS

Xinguang Cao: Writing – original draft; writing – review and editing. **Hongbing Hu:** Software. **Pei-ken Kao:** Methodology. **Brendan Buckley:** Supervision. **Zhipeng Dong:** Data curation; investigation. **Xiuling Chen:** Data curation; formal analysis. **Feifei Zhou:** Data curation; investigation. **Keyan Fang:** Funding acquisition; project administration; supervision; writing – review and editing.

ORCID

Xinguang Cao https://orcid.org/0000-0002-3418-3672
Brendan M. Buckley https://orcid.org/0000-0003-1544-8003
Feifei Zhou https://orcid.org/0000-0002-5450-2239

REFERENCES

Anchukaitis, K.J., Frank, D.C., D'Arrigo, R.D., Andreu-Hayles, L. and Cook, E. (2013) Reconstructed summer temperatures from northwestern North America during the last nine centuries. *Journal of Climate*, 26(10), 3001–3012. https://doi.org/10.1175/jcli-d-11-00139.1.

Anchukaitis, K.J., Wilson, R., Briffa, K.R., Büntgen, U., Cook, E.R., D'Arrigo, R., Davi, N., Esper, J., Frank, D. and Gunnarson, B.E. (2017) Last millennium northern hemisphere summer temperatures from tree rings: part II, spatially resolved reconstructions. *Quaternary Science Reviews*, 163, 1–22. https://doi.org/10.1016/j.quascirev.2017.02.020.

Angeles, G., Bond, B., Boyer, J.S., Brodribb, T., Brooks, J.R. and Burns, M.J. (2004) The-cohesiontension-theory. *New Phytologist*, 163(3), 451–452. https://doi.org/10.1111/j.1469-8137.2004.01142.x.

Björklund, J., Gunnarson, B.E., Seftigen, K., Zhang, P. and Linderholm, H.W. (2015) Using adjusted blue intensity data to attain high-quality summer temperature information: a case study from Central Scandinavia. *The Holocene*, 25(3), 547–556. https://doi.org/10.1177/0959683614562434.

Björklund, J., Seftigen, K., Schweingruber, F., Fonti, P., von Arx, G., Bryukhanova, M.V., Cuny, H.E.C.M., Castagneri, D. and Frank, D.C. (2017) Cell size and wall dimensions drive distinct variability of earlywood and latewood density in northern hemisphere conifers. *New Phytologist*, 216, 728–740. https://doi.org/10.1111/nph.14639.

Björklund, J., von Arx, G., Nievergelt, D., Wilson, R., Van den Bulcke, J., Günther, B., Loader, N.J., Rydval, M., Fonti, P., Scharnweber, T., Andreu-Hayles, L., Büntgen, U., D'Arrigo, R., Davi, N., De Mil, T., Esper, J., Gärtner, H., Geary, J., Gunnarson, B.E., Hartl, C., Hevia, A., Song, H., Janecka, K., Kaczka, R.J., Kirdyanov, A.V., Kochbeck, M., Liu, Y., Meko, M., Mundo, I., Nicolussi, K., Oelkers, R., Pichler, T., Sánchez-Salguero, R., Schneider, L., Schweingruber, F., Timonen, M., Trouet, V., Van Acker, J., Verstege, A., Villalba, R., Wilmking, M. and Frank, D. (2019) Scientific merits and analytical challenges of tree-ring densitometry. *Reviews of Geophysics*, 57, 1–41. https://doi.org/10.1029/2019RG000642.

Björklund, J.A., Gunnarson, B.E., Seftigen, K., Esper, J. and Linderholm, H.W. (2013) Is blue intensity ready to replace maximum latewood density as a strong temperature proxy? A tree-ring case study on Scots pine from northern Sweden. *Climate of the Past Discussions*, 9(5), 5227–5261. https://doi.org/10.5194/cpd-9-5227-2013.

Björklund, J.A., Gunnarson, B.E., Seftigen, K., Esper, J. and Linderholm, H.W. (2014) Blue intensity and density from northern Fennoscandian tree rings, exploring the potential to improve summer temperature reconstructions with earlywood information. *Climate of the Past*, 10, 877–885. https://doi.org/10.5194/cp-10-877-2014

Blake, S., Palmer, J., Björklund, J., Harper, J. and Turney, C. (2020) Palaeoclimate potential of New Zealand Manoao colensoi (*silver pine*) tree rings using blue-intensity (BI). *Dendrochronologia*, 60, 125664. https://doi.org/10.1016/j.dendro.2020.125664.

Briffa, K. and Jones, P. (1990) Basic chronology statistics and assessment. In: Cook, E.R. and Kairiukstis, L.A. (Eds.) *Methods of Dendrochronology: Applications in the Environmental Sciences*. Dordrecht, The Netherlands: Kluwer Academic.

Buckley, B.M., Anchukaitis, K.J., Penny, D., Fletcher, R., Cook, E. R., Sano, M., Nam le, C., Wichienkeeo, A., Minh, T.T. and Hong, T.M. (2010) Climate as a contributing factor in the demise of Angkor, Cambodia. *Proceedings of the National Academy of Sciences of the United States of America*, 107(15), 6748–6752. https://doi.org/10.1073/pnas.0910827107.

Buckley, B.M., Hansen, K., Griffin, K., Schmiege, S., Oelkers, R., D'Arrigo, R., Stahle, D., Davi, N., Nguyen, T.Q.T., Le, C.N. and Wilson, R.J.S. (2018) Blue intensity from a tropical conifer's annual rings for climate reconstruction: an ecophysiological perspective. *Dendrochronologia*, 50, 10–22. https://doi.org/10.1016/j.dendro.2018.04.003.

Buckley, B.M., Stahle, D.K., Luu, H.T., Wang, S.Y.S., Nguyen, T.Q.T., Thomas, P., Le, C.N., Ton, T.M., Bui, T.H. and Nguyen, V.T. (2017) Central Vietnam climate over the past five centuries from cypress tree rings. *Climate Dynamics*, 48(11–12), 3707–3723. https://doi.org/10.1007/s00382-016-3297-y.

Büntgen, U., Frank, D.C., Nievergelt, D. and Esper, J. (2006) Summer temperature variations in the European Alps, a.D. 755–2004. *Journal of Climate*, 19, 5606–5623. https://doi.org/10.1175/JCLI3917.1.

Cai, Q. and Liu, Y. (2013) The June–September maximum mean temperature reconstruction from masson pine (*Pinus massoniana* lamb.) tree rings in Macheng, Southeast China since 1879 AD (in Chinese). *Chinese Science Bulletin*, 58, 169–177.

Campbell, R., Mccarroll, D., Robertson, I., Loader, N.J., Grudd, H. and Gunnarson, B. (2011) Blue intensity in pinus sylvestris tree rings: a manual for a new palaeoclimate proxy. *Tree-Ring Research*, 67, 127–134.

Cao, X., Fang, K., Chen, P., Zhang, P., Björklund, J., Pumijumnong, N. and Guo, Z. (2020) Microdensitometric records from humid subtropical China show distinct climate signals in earlywood and latewood. *Dendrochronologia*, 64, 125764. https://doi.org/10.1016/j.dendro.2020.125764.

Chen, D., Fang, K., Li, Y., Dong, Z., Zhang, Y. and Zhou, F. (2016) Response of Pinus taiwanensis growth to climate changes at its southern limit of Daiyun Mountain, mainland China Fujian Province. *Science China Earth Science*, 59(2), 328–336. https://doi.org/10.1007/sl1430-015-5188-1.

Chen, F., Yuan, Y.J., Wei, W.S., Yu, S.L. and Zhang, T.W. (2012a) Tree ring-based winter temperature reconstruction for Changting, Fujian, subtropical region of Southeast China, since 1850: linkages to the Pacific Ocean. *Theoretical & Applied Climatology*, 109(1–2), 141–151. https://doi.org/10.1007/s00704-011-0563-0.

Chen, F., Yuan, Y.J., Wei, W.S., Yu, S.L. and Zhang, T.W. (2012b) Reconstructed temperature for Yong'an, Fujian, Southeast China: linkages to the Pacific Ocean climate variability. *Global and Planetary Change*, 86-87, 11–19. https://doi.org/10.1016/j.gloplacha.2012.01.005.

Cochard, H. (2006) Cavitation in trees. *Comptes Rendus Physique*, 7(9–10), 1018–1026. https://doi.org/10.1016/j.crhy.2006.10.012.

Cochard, H., Badel, E., Herbette, S., Delzon, S., Choat, B. and Jansen, S. (2013) Methods for measuring plant vulnerability to cavitation: a critical review. *Journal of Experimental Botany*, 64(15), 4779–4791. https://doi.org/10.1093/jxb/ert193.

Cook, E. R. (1985), A Time Series Analysis Approach to Tree Ring Standardization, Ph.D. Thesis, University of Arizona, Tucson, AZ, USA.

Cook, E.R., Briffa, K.R., Shiyatov, S.G. and Mazepa, V. (1990) Tree-ring standardization and growth-trend estimation. In: Cook, E.

R., Kairiukstis, L.A. (Eds.), *Methods of Dendrochronology: Applications in the Environmental Sciences [M]*. Dordrecht: Kluwer Academic Publishers, pp. 104–123.

Cook, E.R., Esper, J. and D'Arrigo, R.D. (2004) Extra-tropical northern hemisphere land temperature variability over the past 1000 years. *Quaternary Science Reviews*, 23(20–22), 2063–2074. https://doi.org/10.1016/j.quascirev.2004.08.013.

Cook, E.R. and Peters, K. (1981) The smoothing spline: a new approach to standardizing forest interior tree-ring width series for dendroclimatic studies. *Tree-Ring Bulletin*, 41, 45–53.

D'Arrigo, R. and Wilson, R. (2006) On the Asian expression of the PDO. *International Journal of Climatology*, 26(12), 1607–1617. https://doi.org/10.1002/joc.1326.

D'Arrigo, R., Wilson, R. and Jacoby, G. (2006) On the long-term context for late twentieth century warming. *Journal of Geophysical Research*, 111(D3), D03103. https://doi.org/10.1029/2005jd006352.

D'Arrigo, R., Wilson, R., Liepert, B. and Cherubini, P. (2008) On the 'divergence problem' in northern forests: a review of the tree-ring evidence and possible causes. *Global and Planetary Change*, 60(3–4), 289–305.

Duan, J., Wang, L., Li, L. and Chen, K. (2010) Temperature variability since A.D. 1837 inferred from tree-ring maximum density of *Abies fabri* on Gongga Mountain, China. *Chinese Science Bulletin*, 55(26), 3015–3022. https://doi.org/10.1007/s11434-010-3182-8.

Duan, J., Zhang, Q.-B., Lv, L. and Zhang, C. (2012) Regional-scale winter-spring temperature variability and chilling damage dynamics over the past two centuries in southeastern China. *Climate Dynamics*, 39(3–4), 919–928. https://doi.org/10.1007/s00382-011-1232-9.

Duan, J., Zhang, Q.B. and Lv, L.-X. (2013) Increased variability in cold-season temperature since the 1930s in subtropical China. *Journal of Climate*, 26(13), 4749–4757. https://doi.org/10.1175/jcli-d-12-00332.1.

Esper, J., Cook, E.R. and Schweingruber, F.H. (2002) Low-frequency signals in long tree-ring chronologies for reconstructing past temperature variability. *Science*, 295(5563), 2250–2253. https://doi.org/10.1126/science.1066208.

Esper, J., Schneider, L., Smerdon, J.E., Schöne, B.R. and Büntgen, U. (2015) Signals and memory in tree-ring width and density data. *Dendrochronologia*, 35, 62–70. https://doi.org/10.1016/j.dendro.2015.07.001.

Fan, Z.-X., Bräuning, A., Yang, B. and Cao, K.-F. (2009) Tree ring density-based summer temperature reconstruction for the central Hengduan Mountains in southern China. *Global and Planetary Change*, 65(1–2), 1–11. https://doi.org/10.1016/j.gloplacha.2008.10.001.

Fritts, H.C. (1976) *Tree Rings and Climate*. London: Academic Press.

Fuentes, M., Björklund J, Seftigen, K., Salo, R, & Aravena, J. C. (2016). A comparison between tree-ring width and blue intensity high and low frequency signals from Pinus sylvestris L. from the Central and Northern Scandinavian Mountains. TRACE - Tree Rings in Archaeology, Climatology and Ecology, Volume 14. Scientific Technical Report 16/04, GFZ German Research Centre for Geosciences, p. 38–43. doi: https://doi.org/10.2312/GFZ.b103-16042

Fuentes, M., Salo, R., Björklund, J., Seftigen, K., Zhang, P., Gunnarson, B., Aravena, J.-C. and Linderholm, H.W. (2017) A 970-year-long summer temperature reconstruction from Rogen, west-Central Sweden, based on blue intensity from tree rings. *The Holocene*, 28(2), 1–13. https://doi.org/10.1177/0959683617721322.

Guo, G., Fang, K., Li, J., Linderholm, H., Li, D., Zhou, F., Dong, Z., Li, Y. and Wang, L. (2018) Increasing intrinsic water-use efficiency over the past 160 years does not stimulate tree growth in southeastern China. *Climate Research*, 76, 115–130.

Harris, I., Osborn, T.J., Jones, P. and Lister, D. (2020) Version 4 of the CRU TS monthly high-resolution gridded multivariate climate dataset. *Scientific Data*, 7, 109. https://doi.org/10.1038/s41597-020-0453-3.

Heeter, K.J., Harley, G.L., Maxwell, J.T., Mcgee, J.H. and Matheus, T.J. (2020) Late summer temperature variability for the southern rocky mountains (USA) since 1735 ce: applying blue light intensity to low-latitude picea engelmannii parry ex engelm. *Climatic Change*, 162, 965–988. https://doi.org/10.1007/s10584-020-02772-9.

Heeter, K.J., Harley, G.L., Maxwell, J.T., Wilson, R.J., Abatzoglou, J.T., Rayback, S.A., Rochner, M.L. and Kitchens, K.A. (2021) Summer temperature variability since 1730 CE across the low-to-mid latitudes of western North America from a tree ring blue intensity network. *Quaternary Science Reviews*, 267, 107064. https://doi.org/10.1016/j.quascirev.2021.107064.

Heeter, K.J., Harley, G.L., Van, D., Gevel, S.L. and White, P.B. (2019) Blue intensity as a temperature proxy in the eastern United States: a pilot study from a southern disjunct population of Picea rubens (Sarg.). *Dendrochronologia*, 55, 105–109.

Holmes, R.L. (1983) Computer-assisted quality control in tree-ring dating and measurement. *Tree-Ring Bulletin*, 44(3), 69–75. https://doi.org/10.1007/BF02656915

Huang, B., Thorne, P.W., Banzon, V.F., Boyer, T., Chepurin, G., Lawrimore, J.H., Menne, M.J., Smith, T.M., Vose, R.S. and Zhang, H.M. (2017) Extended reconstructed sea surface temperature, version 5 (ERSSTv5): upgrades, validations, and intercomparisons. *Journal of Climate*, 30(20), 8179–8205. https://doi.org/10.1175/JCLI-D-16-0836.1.

Huang, J., Guan, X. and Ji, F. (2012) Enhanced cold-season warming in semi-arid regions. *Atmospheric Chemistry and Physics Discussions*, 12, 4627–4653. https://doi.org/10.5194/acpd-12-4627-2012.

Hung, C.W., Hsu, H.-H. and Lu, M.-M. (2004) Decadal oscillation of spring rain in northern Taiwan. *Geophysical Research Letters*, 31, L22206. https://doi.org/10.1029/2004GL021344.

IPCC (2014), Climate change 2014: impacts, adaptation, and vulnerability. Part A: Global and Sectoral Aspects. Contribution of Working Group II to the Fifth Assessment Report of the Intergovernmental Panel on Climate ChangeRep., Cambridge, United Kingdom and New York, NY, USA.

Jacoby, G.C., D'Arrigo, R.D. and Davaajamts, T. (1996) Mongolian tree rings and 20th-century warming. *Science*, 273, 771–773. https://doi.org/10.1126/science.273.5276.771.

Kalnay, E., Kanamitsu, M., Kistler, R., Collins, W.G., Deaven, D., Gandin, L.S., Iredell, M., Saha, S., White, G., Woollen, J., Zhu, Y. and Chelliah, M. (1996) The NCEP/NCAR 40-year reanalysis project. *Bulletin of the American Meteorological Society*, 77, 437–471.

Larsson, L. (2018) CooRecorder and Cdendro programs of the CooRecorder/Cdendro package version 7.6, http://www.cybis.se/forfun/dendro/ [Accessed 10th October 2018].

Larter, M., Pfautsch, S., Domec, J.C., Trueba, S., Nagalingum, N. and Delzon, S. (2017) Aridity drove the evolution of extreme embolism resistance and the radiation of conifer genus Callitris. *The New Phytologist*, 215(1), 97–112. https://doi.org/10.1111/nph.14545.

Li, M., Huang, L., Yin, Z.-Y. and Shao, X. (2017) Temperature reconstruction and volcanic eruption signal from tree-ring width and maximum latewood density over the past 304 years in the southeastern Tibetan plateau. *International Journal of Biometeorology*, 61(11), 2021–2032. https://doi.org/10.1007/s00484-017-1395-0.

Li, M., Wang, L., Fan, Z.-X. and Shen, C. (2015) Tree-ring density inferred late summer temperature variability over the past three centuries in the Gaoligong Mountains, southeastern Tibetan plateau. *Palaeogeography, Palaeoclimatology, Palaeoecology*, 422, 57–64. https://doi.org/10.1016/j.palaeo.2015.01.003.

Li, Y., Fang, K., Cao, C., Li, D., Zhou, F., Dong, Z., Zhang, Y. and Gan, Z. (2016) A tree-ring chronology spanning 210 years in the coastal area of southeastern China and its relationship with climate change. *Climate Research*, 67(3), 209–220. https://doi.org/10.3354/cr01376.

Liang, E., Shao, X. and Qin, N. (2008) Tree-ring based summer temperature reconstruction for the source region of the Yangtze River on the Tibetan plateau. *Global and Planetary Change*, 61, 313–320. https://doi.org/10.1016/j.gloplacha.2007.10.008.

Liang, H., Lyu, L. and Wahab, M. (2016) A 382-year reconstruction of august mean minimum temperature from tree-ring maximum latewood density on the southeastern Tibetan plateau, China. *Dendrochronologia*, 37, 1–8. https://doi.org/10.1016/j.dendro.2015.11.001.

Macdonald, G.M. and Case, R.A. (2005) Variations in the Pacific decadal oscillation over the past millennium. *Geophysical Research Letters*, 32(8), L08703. https://doi.org/10.1029/2005GL022478.

Mann, M.E. and Lees, J. (1996) Robust estimation of background noise and signal detection in climatic time series. *Climate Change*, 33, 409–445. https://doi.org/10.1007/BF00142586.

McCarroll, D., Loader, N.J., Jalkanen, R., Gagen, M.H., Grudd, H., Gunnarson, B.E., Kirchhefer, A.J., Friedrich, M., Linderholm, H.W., Lindholm, M., Boettger, T., Los, S.O., Remmele, S., Kononov, Y.M., Yamazaki, Y.H., Young, G.H.F. and Zorita, E. (2013) A 1200-year multiproxy record of tree growth and summer temperature at the northern pine forest limit of Europe. *The Holocene*, 23(4), 471–484. https://doi.org/10.1177/0959683612467483.

McCarroll, D., Pettigrew, E., Luckman, A., Guibal, F. and Edouard, J.-L. (2002) Blue reflectance provides a surrogate for latewood density of high-latitude pine tree rings. *Arctic, Antarctic, and Alpine Researc*, 34, 450–453. https://doi.org/10.1080/15230430.2002.12003516.

Moberg, A., Sonechkin, D.M., Holmgren, K., Datsenko, N.M. and Karle´n, W.R. (2005) Highly variable northern hemisphere temperatures reconstructed from low- and high-resolution proxy data. *Nature*, 433(7026), 613–617. https://doi.org/10.1038/nature0365.

Neukom, R., Steiger, N., Gómez-Navarro, J.J., Wang, J. and Werner, J.P. (2019) No evidence for globally coherent warm and cold periods over the preindustrial common era. *Nature*, 571, 550–554. https://doi.org/10.1038/s41586-019-1401-2.

Pepin, N., Bradley, R.S., Diaz, H.F., Baraer, M., Cáceres, B., Forsythe, N., Fowler, H.J., Greenwood, G., Hashmi, M.Z.u.R., Liu, X.D., Miller, J.R., Ning, L., Ohmura, A., Palazzi, E., Rangwala, I., Schöner, W., Severskiy, I., Shahgedanova, M., Wang, M.B., Williamson, S.N. and Yang, D. (2015) Elevation-dependent warming in mountain regions of the world. *Nature Climate Change*, 5(5), 424–430. https://doi.org/10.1038/nclimate2563.

Popa, I. and Bouriaud, O. (2014) Reconstruction of summer temperatures in eastern Carpathian Mountain. *International Journal of Climatology*, 34, 871–880. https://doi.org/10.1002/joc.3730.

Rossi, S., Deslauriers, A., Anfodillo, T., Morin, H., Saracino, A., Motta, R. and Borghetti, M. (2006) Conifers in cold environments synchronize maximum growth rate of tree-ring formation with day length. *The New Phytologist*, 170(2), 301–310. https://doi.org/10.1111/j.1469-8137.2006.01660.x.

Rydval, M., Gunnarson, B.E., Loader, N.J., Cook, E.R., Druckenbrod, D.L. and Wilson, R. (2016) Spatial reconstruction of Scottish summer temperatures from tree rings. *International Journal of Climatology*, 37(3), 1540–1556. https://doi.org/10.1002/joc.4796.

Rydval, M., Larsson, L.-Å., McGlynn, L., Gunnarson, B.E., Loader, N.J., Young, G.H.F. and Wilson, R. (2014) Blue intensity for dendroclimatology: should we have the blues? Experiments from Scotland. *Dendrochronologia*, 32(3), 191–204. https://doi.org/10.1016/j.dendro.2014.04.003.

Rydval, M., Loader, N.J., Gunnarson, B.E., Druckenbrod, D.L., Linderholm, H.W., Moreton, S.G., Wood, C.V. and Wilson, R. (2017) Reconstructing 800 years of summer temperatures in Scotland from tree rings. *Climate Dynamics*, 49(9–10), 2951–2974. https://doi.org/10.1007/s00382-016-3478-8.

Sano, M., Buckley, B.M. and Sweda, T. (2009) Tree-ring based hydroclimate reconstruction over northern Vietnam from Fokienia hodginsii: eighteenth century mega-drought and tropical Pacific influence. *Climate Dynamics*, 33(2–3), 331–340. https://doi.org/10.1007/s00382-008-0454-y.

Schongart, J., Orthmann, B., Hennenberg, K.J., Porembski, S. and Worbes, M. (2006) Climate-growth relationships of tropical tree species in West Africa and their potential for climate reconstruction. *Global Change Biology*, 12(7), 1139–1150. https://doi.org/10.1111/j.1365-2486.2006.01154.x.

Seftigen, K., Fuentes, M., Ljungqvist, F.C. and Björklund, J. (2020) Using blue intensity from drought-sensitive Pinus sylvestris in Fennoscandia to improve reconstruction of past hydroclimate variability. *Climate Dynamics*, 55, 579–594. https://doi.org/10.1007/s00382-020-05287-2.

Serreze, M.C. and Barry, R.G. (2011) Processes and impacts of Arctic amplification a research synthesis. *Global and Planetary Change*, 77, 85–96. https://doi.org/10.1016/j.gloplacha.2011.03.004.

Shi, J., Cook, E.R., Lu, H., Li, J., Wright, W.E. and Li, S. (2010) Tree-ring based winter temperature reconstruction for the lower reaches of the Yangtze River in Southeast China. *Climate Research*, 41, 169–176. https://doi.org/10.3354/cr00851.

Shi, J., Li, L., Han, Z., Hou, X. and Shi, S. (2015) Tree-ring width based June-September temperature reconstruction and its teleconnection with PDO and ENSO in mount Daowu, Hunan Province. *Quaternary Sciences*, 35, 1155–1164 (in Chinese).

Tingley, M.P. and Huybers, P. (2013) Recent temperature extremes at high northern latitudes unprecedented in the past 600 years. *Nature*, 496, 201–205. https://doi.org/10.1038/nature11969.

Torrence, C. and Compo, G.P. (1998) A practical guide to wavelet analysis. *Bulletin of the American Meteorological Society*, 79(1), 61–78. https://doi.org/10.1175/1520-0477(1998)07960;0061:apgtwa62;2.0.co;2.

Trouet, V. and Van Oldenborgh, G.J. (2013) Knmi climate explorer: a web-based research tool for high-resolution paleoclimatology. *Tree-Ring Research*, 69(1), 3–13. https://doi.org/10.3959/1536-1098-69.1.3.

Tyree, M.T. and Zimmermann, M.H. (2002) *Xylem Structure and the Ascent of Sap*. Berlin, Germany: Springer.

Wang, B., Wu, R. and Fu, X. (2000) Pacific–east Asian teleconnection: how does ENSO affect east Asian climate? *Journal of Climate*, 13, 1517–1536.

Wang, B. and Zhang, Q. (2002) Pacific– east Asian teleconnection. Part II: How the Philippine Sea anomalous anticyclone is established during El Niño development. *Journal of Climate*, 15, 3252–3265.

Wang, J., Yang, B. and Ljungqvist, F.C. (2015) A millennial summer temperature reconstruction for the eastern Tibetan plateau from tree-ring width. *Journal of Climate*, 28(13), 5289–5304. https://doi.org/10.1175/jcli-d-14-00738.1.

Wang, L., Fang, K., Chen, D., Dong, Z., Zhou, F., Li, Y., Zhang, P., Ou, T., Guo, G., Cao, X. and Yu, M. (2018) Intensified variability of the El Niño–southern oscillation enhances its modulations on tree growths in southeastern China over the past 218 years. *International Journal of Climatology*, 38, 5293–5304. https://doi.org/10.1002/joc.5730.

Wigley, T.M.L., Briffa, K.R. and Jones, P.D. (1984) On the average value of correlated time series, with applications in dendroclimatology and hydrometeorology. *Journal of Climatology & Applied Meteorology*, 23(2), 201–213.

Wilson, R., Anchukaitis, K., Andreu-Hayles, L., Cook, E., D'Arrigo, R., Davi, N., Haberbauer, L., Krusic, P., Luckman, B., Morimoto, D., Oelkers, R., Wiles, G. and Wood, C. (2019) Improved dendroclimatic calibration using blue intensity in the southern Yukon. *The Holocene*, 29(11), 1817–1830. https://doi.org/10.1177/0959683619862037

Wilson, R., D'Arrigo, R., Andreu-Hayles, L., Oelkers, R., Wiles, G., Anchukaitis, K. and Davi, N. (2017) Experiments based on blue intensity for reconstructing North Pacific temperatures along the Gulf of Alaska. *Climate of the Past*, 13(8), 1007–1022. https://doi.org/10.5194/cp-13-1007-2017.

Wilson, R., Rao, R., Rydval, M., Wood, C., Larsson, L.-Å. and Luckman, B.H. (2014) Blue intensity for dendroclimatology: the BC blues: a case study from British Columbia, Canada. *The Holocene*, 24(11), 1428–1438. https://doi.org/10.1177/0959683614544051.

Wodzicki, T.J. (1971) Mechanism of xylem differentiation in *Pinus silvestris L. Journal of Experimental Botany*, 22(3), 670–687. https://doi.org/10.1093/jxb/22.3.670.

Yadav, R.R., Braeuning, A. and Singh, J. (2011) Tree ring inferred summer temperature variations over the last millennium in western Himalaya, India. *Climate Dynamics*, 36, 1545–1554. https://doi.org/10.1007/s00382-009-0719-0.

Yang, M.Q. (2021) Study on annual growth dynamics of xylem of Pinus massoniana of different ages in Daiyun Mountain. Master Thesis. Fuzhou: Fujian Normal University, 2021 (in Chinese).

Zhang, Y., Fang, K.Y., Zhou, F.F., Dong, Z.P., Gan, Z.F. and Li, D. W. (2016) A study on the inter-annual latewood growth of *Pinus massoniana* in Fuzhou. *Journal of Subtropical Resources and Environment*, 11(1), 59–64 (in Chinese).

Zhou, X.J., Zhao, P. and Liu, G. (2009) Asian-Pacific oscillation index and variation of east Asian summer monsoon over the past millennium. *Chinese Science Bulletin*, 54, 3768–3771. https://doi.org/10.1007/s11434-009-0619-z.

Zhu, H., Zheng, Y., Shao, X., Liu, X., Xu, Y. and Liang, E. (2008) Millennial temperature reconstruction based on tree-ring widths of Qilian juniper from Wulan, Qinghai Province, China. *Chinese Science Bulletin*, 53(24), 3914–3920. https://doi.org/10.1007/s11434-008-0400-8.

SUPPORTING INFORMATION

Additional supporting information may be found in the online version of the article at the publisher's website.

How to cite this article: Cao, X., Hu, H., Kao, P., Buckley, B. M., Dong, Z., Chen, X., Zhou, F., & Fang, K. (2022). Improved spring temperature reconstruction using earlywood blue intensity in southeastern China. *International Journal of Climatology*, 1–17. https://doi.org/10.1002/joc.7585